On the transformation behaviour of NiTi particulate reinforced AA2124 composites

R. R. Thorat [a], D. D. Risanti [b,*], D. San Martin [c], G. Garces [d], P. E. J. Rivera Díaz del Castillo [a], S. van der Zwaag [a]

[a] *Fundamentals of Advanced Materials Group, Faculty of Aerospace Engineering, Delft University of Technology, Kluyverweg 1, 2629 HS Delft, The Netherlands*

[b] *Materials for Innovation Institute, Mekelweg 2, 2628 CD Delft, The Netherlands*

[c] *MATERALIA group, Department of Physical Metallurgy, National Center for Metallurgical Research (CENIM-CSIC), Av. Gregorio del Amo 8, 28040 Madrid, Spain*

[d] *Department of Physical Metallurgy, National Center for Metallurgical Research (CENIM-CSIC), Av. Gregorio del Amo 8, 28040 Madrid, Spain*

Abstract

The transformation behaviour of AA2124 alloys reinforced NiTi particulates of 10 vol pct and 20 vol pct has been studied by differential scanning calorimetry (DSC), thermoelectric power (TEP) and internal friction (IF). Addition of NiTi particulates increase the damping capacity as well as the precipitation kinetics of AA2124 composites with respect to the base AA2124. Heat treatments performed to change the matrix condition do not alter the transformation significantly, other than homogeneising the Al level in the particulates, which is present due to the preceeding extrusion treatment. The presence of Al in NiTi stabilizes the R-phase transformation but the M_s remains stable.

Preprint submitted to Journal of Alloys and Compounds *19 September 2008*

Key words: composite materials, shape memory alloy, calorimetry, mechanical spectroscopy, thermoelectric

1 Introduction

Metal matrix composites (MMCs) are compound material whose microstructure consists of a metallic alloy into which a particular reinforcing component is introduced. MMCs offer advantages in applications where low density, high strength and high stiffness are a primary concern. Among the various types of composites, the family of discontinuous MMCs containing particulates, whiskers, nodules and platelets, are favored because they offer improvements to the mechanical properties those of the the monolithic alloy while remaining relatively easily deformable. The particulate reinforced MMCs are particularly attractive because they exhibit near isotropic properties compared to the continuously reinforced counterparts [1, 2]. The availability of various types of reinforcements at competitive costs, the feasibility of mass production and high damping capacity [3, 4] make this type of MMC more attractive. However, these materials may suffer from inhomogeneous distribution, size or shape of particulate, low ductility, inadequate fracture toughness and inferior fatigue crack growth performance compared to that of the matrix [5, 6].

To optimize the mechanical and physical properties in particular its damping conditions and damage tolerance of such particulate reinforced MMCs, one can

* Corresponding author. Address: Kluyverweg 1, 2629 HS Delft, The Netherlands. Tel.:+31 15 278 8621; fax: +31 15 278 4472
Email address: d.d.risanti@tudelft.nl (D. D. Risanti).

utilize shape memory alloy as reinforcement. Shape memory alloys (SMA) have received great attention because of their shape memory effect (SME) and many investigations are conducted on their basic performance and applications. To date SMA fibers have been added to soft and ductile metal or polymer matrices *e.g.*[7–10], to improve the mechanical properties making use of the reversable transformation of SMA from martensite to austenite state. The transformation in a compression can result stress in the matrix, which in turn enhances the mechanical properties, such as yield stress [9–12], fracture toughness [13, 14], suppression of crack growth [15, 16] and fatigue [11, 17]. Two SMAs which generate large amounts of strain and are capable of generating a large force upon transformation back to the austenitic phase are NiTi alloys and Cu-based alloys. Copper-based SMAs are particularly interesting because of their low cost and relative ease of processing. However, copper alloys posses low strength compared to NiTi alloys and also exhibits a degradation of shape memory capacity when thermally cycled [18]. On the other hand, NiTi alloys tend to be more thermally stable and have a lower density, higher yield and ultimate tensile strength, and corrosion resistant than the Cu-based alloys [19].

The high temperature austenite phase of NiTi alloys has B2 type ordered cubic structure that transforms to B19 monoclinic martensite phase by cooling or applied stress. The transformation behavior in pure systems is known to be sensitive not only to compositional variation [20, 22–26], heat treatment [27, 28] and applied stress [29] but also to transformation cycles [26, 30, 58]. So far, the transformation behaviour has been studied using different tools, such as electrical resistivity *e.g.*[22, 31], differential scanning calorimetry (DSC) *e.g.*[27, 28], internal friction measurement [22, 23, 30, 32, 33], magnetic sus-

ceptibility [34] and thermoelectric power [31]. The transformation behaviour of NiTi embedded in a precipitation hardenable aluminium alloy has not been investigated yet, as earlier work on such systems was aimed at tailoring the mechanical properties [7–9, 11, 12, 35, 36] and processing route [12, 36].

In the present work the transformation behaviour of NiTi particulates embedded in AA2124 matrix was studied. Particular emphasis has been placed on ascertaining the roles of matrix microstructure and precipitate states produced by heat treatments, as the transformations may be sensitively affected by the surrounding matrix microstructure.

2 Experimental Methods

2.1 Fabrication of NiTi SMA-AA 2124 Composite and Heat Treatments

The material used in the present experiments was a powder metallurgycally processed AA2124 composite, reinforced with 10 and 20 vol.% NiTi particulates fabricated at Centro Nacional de Investigaciones Metalúrgicas (CENIM-CSIC). The nominal elemental composition of the atomized AA2124 powder with the average diameter of 32 μm from Alpoco is given in Table 1. The atomized NiTi powder (Ni 55.7 wt.% and average diameter of 30 μm) from Nanoval was used as the reinforcement.

Billets with a diameter of about 10 mm containing 0, 10 and 20 Vol. % NiTi particulates were produced by hot extrusion. During processing the air tight cans were kept at 773 K in furnace for 90 minutes before hot extrusion to soften the powders and improve their extrudability. The extrusion rate used was 0.4

mm/s with a starting pressure around 440 MPa. The extrusion temperature was maintained at 753 K.

To study the effect of matrix microstructure condition on the martensitic transformation behaviour of the embedded NiTi particulates, the composite samples were subjected to two different heat treatments: solutionising at 768 K for 1 hour followed by water quench to obtain a soft matrix, hereafter termed as *SOL* and solutionising at 768 K for 1 hour followed by water quench and subsequently aged for 12 hours at 463 K to achieve an optimum precipitate amount and maximum hardness in the matrix, designated as *AGED*.

2.2 Characterization techniques

The microstructure of the base AA2124 alloy and the composites were studied by means of light optical microscopy (LOM). For that purpose, the specimens were ground, polished and etched using Kellers reagent. The NiTi particulate's morphology, composition and its spatial distribution in the composite matrix were further analyzed by scanning electron microscopy (SEM) using a FEG-SEM JEOL-7500F equipped with EDX Thermo-Noran.

Thermal transformation effects were measured in a Sapphire-Cell Perkin Elmer DSC on all sample conditions. The as-extruded composite and NiTi bulk samples were cut by spark erosion in a cylindrical form with a weight of about 150 mg. The scans were carried out in an argon gas atmosphere with a heating/cooling rate of 2 K/min. The heat flow was recorded in a range of temperatures between 100 K and 350 K. To study the changes in the precipitation reactions in the aluminium matrix due to the presence of NiTi particulate,

the scans were also performed between 300 and 723 K with a heating rate of 10 K/min. Each DSC scan was repeated at least 2 to 3 times to confirm the reproducibility of the results.

The scanning thermoelectric power (TEP) measurements were undertaken with an Anatech Scanning TEP instrument. Description of this equipment can be found elsewhere [37]. Samples with dimensions 70 mm x 2 mm x 1 mm were employed. A temperature difference of 10 K between the two ends of the specimen was used in order to generate the Seebeck effect. The thermoelectric voltage of the specimen with respect to the aluminum reference was measured as a function of temperature during heating/cooling at 2 K/min in a range of temperatures between 100 K and 350 K.

Internal friction (IF) measurements were used to characterize the damping capacity of the composites. The measurement was performed using an inverted free torsion pendulum with a constant strain amplitude of 5 x 10^{-5} in all studied samples. Samples with a dimension of 58 mm x 4 mm x 1 mm were cooled/heated in a He atmosphere between 100 K and 600 K at a rate of 2 K/min. At least two independent test runs were performed to check for full reproducibility.

3 Results

3.1 Materials

Figure 1 shows a central cross section of as-extruded composites. A number of particulate clusters are present and a significant amount of side-by-side par-

ticulate contact occurs within transverse planes. The scanning electron images in Figure 1 show diffused interfacial products, which were identified as Al_3Ti (grey) and Al_3Ni (light grey) as indicated in detail in Figure 1c. Those intermetallics layers were also observed in NiTi fiber reinforced AA6061 during processing at temperatures between 773 K and 873 K [10]. The NiTi particulate interfaces are smoother compared to the intermetallics layers indicating that Al atoms diffuse from the matrix into the particulates. The diffusion of Al lead to an Al-rich layer inside NiTi particle as indicated in Fig. 1c. The presence of Al in the interior of NiTi modifies the NiTi particulate composition to a lower Ni concentration due to Al substitutes Ni. In addition, the as-received materials show constituents in the size of about 1 to 2 microns which were mainly found on the grain boundaries and dispersoids in the size of about 0.3 microns within the grains. Only few pores were found particularly in the NiTi containing materials. *SOL* and *AGED* treatment results in homogenization of Al inside the NiTi particulates, as evidenced that the NiTiAl layers inside NiTi particulate disappear after those treatments. The average Ni/Ti ratio of *SOL* and *AGED* was found to be about 0.910 and 0.907, respectively. This value was determined by EDX after averaging the results of several particles.

3.2 Differential Scanning Calorimetry Study

A. Scanning between 300 and 700 K

The DSC thermograms of the composites revealed a change in the precipitation kinetics of AA2124 as shown in Figure 2. DSC thermograms of AA2124 shows the general features of this precipitate hardenable alloy [38–40]: an exotherm

between 300 K and 423 K due to the formation of GPB zones (Peak 1); an endotherm between 423 K and approximately 583 K due to the dissolution of GPB zones (Peak 2); an exotherm between 518 K and 583 K due to the formation of S'(Peak 3) followed by a broad endothermic above 583 K due to the dissolution of S' precipitate (Peak 4). Overall, the presence of NiTi particulates does not principally change the precipitation sequence, but some aspects of the reactions are altered.

The *SOL* materials generally exhibit the expected prominent reaction peaks due to the solute supersaturation in the matrix. However, an additional dip (Af) slightly above 300 K was observed in NiTi containing materials, which is attributed to the austenitic transformation of NiTi particulates. Apart from that, the GPB zone formation peak (Peak 1) is still visible in the composites containing 10 % with the smaller enthalpy compared to AA2124 indicating the activation energy of GPB zone formation has increased due to the presence of dislocations in the matrix which act as vacancies sink. Consequently, the dissolution of GPB zone is also smaller (Peak 2). A limited amount of S' precipitate has been formed as indicated by a broad and weak Peak 3. Increasing NiTi to 20 % results in an inhibition of GPB zone formation (Peak 1) and disappearance of GPB zone dissolution (Peak 2). No Peak 3 was observed which indicates that a greater number of dislocations in the matrix provide preferential nucleation sites for S' precipitate and thereby, fewer precipitates may form during scanning.

AGED treatment results in flat thermal curves for the composite materials, indicating the S' precipitation reaction has been completed due to this heat treatment, whereas the unreinforced AA2124 still exhibits a dissolution dip (Peak 2) which refers to the presence of several over-critical sized GPB zones

even after long term aging [40] and a weak and broad peak of S' precipitate (Peak 3).

The comparison of the curves corresponding to the three different materials in the *SOL* and *AGED* conditions indicates that the aluminium matrix microstructure has been altered by the heat treatments and that the NiTi particulates influence the precipitation/dissolution kinetics of GP zones and S' phase. The presence of the NiTi particulates accelerates the precipitation reactions in the aluminium matrix. The small dip (Af) as indicative of the martensite to austenite transformation in NiTi containing composites shifts slightly in temperature position.

B. Scanning between 350 and 100 K

Figure 3 shows a set of DSC scans displaying the NiTi particulates transitions obtained upon cooling and heating. In all heat treament conditions, the unreinforced AA2124 reveals no exothermal and/or endothermal peak during scanning heating and cooling between 350 K and 100 K. The change in reinforcement volume fraction is proportional to transformation enthalpies. In NiTi containing materials, both heat treatments show a typical transformation of NiTi. On cooling from 350 K to 100 K, two exothermic transitions are present corresponding to Austenite → R-phase (peak R) and R-phase → Martensite (peak M) transitions.

Upon heating the heat flow curve is characterised by only one endothermic transition (peak A) related to the formation of Austenite phase. All start, peak and finish transition temperatures were determined using a standard line crossing technique and the results along with enthalpy of transformations

are listed in Table 2. The A→M transformation indicated in Table 2 comprises of A→R and R→M transformations. As can be seen from Table 2, the heat of transformation for A→M is approximately equal to that of M→A. *AGED* treatment produces a similar behaviour both in heating and in cooling as shown by *SOL* treatment.

3.3 Thermoelectric Power Study

Changes in temperature dependence of the thermoelectric power (TEP) for the composites examined were observed to be similar to those observed with DSC (Figure 4). The unreinforced alloy showed the same features as wrought aluminium alloys [41]. The temperature dependence of the TEP is indicative of the amount of solute in the matrix. Solution treated posseses the maximum solute level and subsequent aging at 463 K results in a lower value because of solute consumption for precipitation [42, 43]. The TEP signals of the NiTi containing materials show an abrupt change in the vicinity of the austenitic to martensitic phase transition for all heat treatment conditions. R-phase transformation could not be resolved in TEP due to its lack of significant energy to alter TEP [31]. Generally, the NiTi reinforcement in AA2124 affects the overall TEP signal in three ways:

(1) *Solute level*: The NiTi reinforcement shifts the overall TEP value to higher levels. The shift towards higher TEP values is primarily due to the high TEP value of NiTi itself ($\backsim$10 μV/K [31]). Secondly, for the supersaturated state of the AA2124 matrices the TEP value is also raised. Since the TEP of MMCs follows the rule of mixtures [44] both factors contribute to the nett TEP signal.

(2) *Austenitic-martensitic transformation* is responsible for a hysteresis effect which becomes more noticeable in the composite for high NiTi fraction. The abrupt change in the TEP upon transformation is related to changes in the density of states (DOS) near the Fermi level, with the DOS at the Fermi level being lower for the martensitic than for the austenitic state [31, 34] due to lattice instabilities. Based on the strong transition presented in Figure 4, the austenitic and martensitic start and finish temperatures (A_s, A_f, M_s and M_f) were easily determined. The results are summarized in Table 3.

(3) *Electron diffusion-phonon drag effects on temperature dependence of TEP*: From resistivity measurements [31] it is known that NiTi possesses a strong disorder scattering which leads to suppression of thermoelectric phonon drag. Therefore, the TEP of NiTi decreases towards $S \approx 0$ at $T \approx 0K$ with the slope $\frac{dS}{dT}$ increasing as T decreases. In aluminium alloys, the effect of phonon drag is not negligible at low temperatures and remains high [41]. As a result the temperature dependence of TEP at low temperatures decreases with increasing NiTi fraction.

3.4 Internal Friction Study

A. High temperature damping behaviour (300 K - 600 K)

Figure 5 shows the temperature dependent internal friction (TDIF) spectrum recorded during a continuous heating at 2 K/min up to 600 K, for the three different materials studied, in the *SOL* and *AGED* conditions. In the *SOL* condition, the curves shift towards higher damping the higher the NiTi volume fraction present in the composite, being this shift in damping capacity higher, the higher the temperature (Fig. 5a). The frequency of free oscillation

decreases monotonously with temperature while the background damping increases. A similar increase in internal friction intensity was also reported in AlCu-Al_2O_3 and Al/NiTi-fiber reinforced composites, in which the authors related the increase in damping to the presence of a higher density of mobile dislocations [45] and the stiffness difference between NiTi and the matrix [9].

As can be seen in Figure 5a, the unreinforced sample exhibits a well developed peak which corresponds to Zener peak (P1 around 500 K), characteristic for Cu retained in solid solution. Another low intensity peak which is attributed to the GPB zone formation [45] was detected in the unreinforced sample at a temperature about $\backsim$350 K, but disappeared on subsequent cooling. Addition of NiTi to the aluminium matrix resulted in a strong increase in damping intensity and appearance of broad peak P2, which is associated with the presence of S phase. As shown by the DSC data, the kinetics of precipitation in the composite materials is faster than that of unreinforced one. A decrease in IF which is associated with the end of martensite-austenite transition was observed at temperature range of 325 - 340 K for the NiTi containing materials. A related drop in apparent heat capacity was observed in the DSC (see: Figure 2).

Figure 5b displays that *AGED* treatment did not change the dependency of damping capacity and frequency on NiTi volume fraction. The IF is systematically higher in the composite than in the unreinforced alloy. Obviously, all spectras exhibit only P2, as indicative of S' precipitation. The increase of frequency is more pronounced in the composite than in the unreinforced alloy, which confirms the faster hardening of the composite.

B. Low temperature damping behaviour (350 K - 100 K)

Figure 6 shows how internal friction between 350 and 100 K changes with prior heat treatment as well as NiTi particulates volume fraction. In general, the peak intensity is proportional to the NiTi volume fraction. Unreinforced AA2124 showed no damping peak in this low temperature regime. Upon cooling (Fig. 6a) all NiTi composites exhibited three peaks of P_R and P_M, which are ascribed to austenite→R-phase and R-phase→martensite, respectively. The fact that peak P_{rel} was not observed in the unreinforced material relates it to the presence of NiTi particulates. This peak has been observed earlier in aluminium matrix composites and NiTi SMAs and has been related in both cases to the presence of dislocations [30, 32, 45–47]. The (A→R) transformation is characterised by a sharp peak (P_M) accompanied by a drop in the apparent shear modulus (Fig. 6b), which is indicative of a relaxation process whose relaxation time is strongly temperature dependence. The P_R peak is located as a shoulder of P_M peak. Upon heating (Fig. 6c) only two well-developed peaks were observed, namely P_{rel} and P_A. As for the A→R transformation, the reverse M→A transformation corresponded to a minimum in the oscillation frequency (Fig. 6d). Taking into account that f is proportional to shear modulus G, the discontinuity equals to derivative of f-T and hence the discontinuity in f^2-T curve clearly proves that the transformation is a first order phase transformation. The effects of *SOL* and *AGED* treatments on NiTi particulates transformation temperatures are summarized in Table 4. These results show that the higher the volume fraction of NiTi, the stronger the influence of the heat treatments on the transformation temperatures.

4 Discussion

4.1 Influence of the NiTi particulates on precipitation in the aluminium matrix and the damping capacity at higher temperatures (300 K - 600 K)

For metal matrix composites, its thermal behaviour differs from that of the unreinforced matrices due to the presence of the reinforcements, the presence of the interface layer between particles and matrices and the effect of the particles on processes taking place in the matrices. The DSC results (Fig. 2) show that the presence of NiTi particulates causes an acceleration in aging kinetics. Such acceleration in precipitation kinetics for identical heat treatments has been reported earlier [39, 45, 48–50]. However, it was found that this acceleration depends on the aging temperature and became absent for aging temperature below 423 K [50]. Acceleration of S' precipitate formation is due to the presence of a network of dislocations that can act as high diffusivity paths in the composite for Cu diffusion[39, 45, 48, 50]. The sources of the dislocations itself come from particularly the renforcement-matrix interfaces and its generation due to the different in coefficient of thermal expansion between Al matrix (23.6 μm/K) and the NiTi (6-11.0 μm/K)[12]. The number density of dislocations generated depends on the size, volume fraction [51] and particulate distribution [52]. Moreover, in general the ageing kinetics in powder metallurgically processed materials is known to be faster compared to the cast ones [38, 49]. Despite the increased kinetics of S' precipitate formation, the presence of dislocation alters the GPB zones formation in a different way as depicted in Fig. 2 for *SOL* samples. GPB zones are coherent precipitates which form at low temperatures, and whose growth is controlled by Cu and

Mg atoms diffusion in the matrix. Cu diffusion can be strongly favoured by a vacancy supersaturation in the lattice, since the most favoured mechanism for diffusion in substitutional alloys is the solute-vacancy exchange [53]. Accordingly, an enhanced dislocation density in AA2124 matrix can have effects on GPB zones formation by changing the degree of vacancy supersaturation, where profuse dislocations act as vacancy sinks leading to a deceleration or inhibition of GPB zones formation.

The Al_3Ti and Al_3Ni intermetallics formed at the NiTi-matrices interface can also contribute to the damping capacity. Their CTE values are unknown, it is likely that the CTE of intermetallics compound is lower than that of Al. Therefore, during quenching additional tensile residual stresses are expected in the base material, which may contribute to the damping capacity. However, from the point of view of the mechanical properties of the composite, the presence of such intermetallics is undesirable as it lowers the interfacial bond strength of aluminium with NiTi and it becomes the key sites for fracture initiation and failure [3, 8].

AGED treatment produces, apparently, an increase in damping capacity at high temperatures (325 - 600 K) (Fig. 5b). The reduction of the peak height indicates the amount of Cu in solid solution being consumed to produce precipitates and most likely that the already existed S' precipitates partly transformed into S precipitates along with loss of coherency [54].

4.2 The effects of annealing conditions on NiTi transformation characteristics

As mentioned earlier, phase transformations (A→R, R→M, M→A) taking place in the NiTi particulates of these materials are sensitive to several factors [58], *i.e.* Ni-content, heat treatment, thermal cycling and substitution of Ni or Ti by a third element. Due to Al diffusion into the NiTi particulates during preheating treatment prior to the extrusion, the amount of Al inside NiTi particulates is about 10 at.%. After heat treatment the remaining Al inside NiTi was 2.3 to 3.7 at.%. This shifts the Ni-content to about ∼46-47 at.% which lays on the range where the M_s is stable against Ni-content variation [55]. The addition of Al to NiTi has been reported to promote the formation of the intermediate R-phase, to shift transformation temperatures to lower values with increasing thermal cycles and to broaden the transformation temperature range of these transformations also with increasing thermal cycles [24]. In Figures 3 and 6a-b, it is shown that IF and DSC detect the formation of R-phase in the composites, although earlier works would suggest that in NiTi alloys with the composition used in this work, this phase should not be detected [22, 23].

The temperature at which solution treatment was undertaken affects the NiTi transformation behaviour. It is known that the heat treatment performed on equiatomic NiTi between 673 and 873 K causes a multistep transformation [27, 28]. The appearance of R-phase is believed due to the formation of $Ti_{11}Ni_{14}$ or Ni_3Ti_4 precipitates during aging. The subsequent aging at 463 K for 12 hours may have no effect on those precipitates, since those phases are already stable at 463 K and the presence of Al in the NiTi particulates is known to

retard the nucleation and growth rate of $Ti_{11}Ni_{14}$ [56]. As a result, the amount of $Ti_{11}Ni_{14}$ or Ni_3Ti_4 in NiTi particulates should be comparable for both the *SOL* and *AGED* conditions.

The formation of the R-phase directly from austenite can be observed by DSC and IF experiments (Figures 3, 6a and b). The heat effect associated with R→M transformation is stronger as compared to the A→R transformation (Fig. 3a). In the TDIF spectra, the relaxation strength of peak P_M is larger than that of P_R (Fig. 6a), which is attributable to the presence of twin boundaries in the B19' martensite and R-phase [57]. The movement of interfaces (twin and intervariant boundaries) and/or the twin dislocations forming the interfaces as well as the movement of the twin boundaries leads to frictional work, which is dissipated as heat in the system causes the high damping. Apparently the heat of transformation associated with martensitic transformation is about ten times larger than that associated with the R-phase transformation [58].

As can be seen in Fig. 6 and has been discussed before, the internal friction spectrum of NiTi at low temperatures shows four different peaks, three of them (P_M, P_R, P_A) are associated to the martensitic transformation. It is well known that there are three main contributors to these three internal friction peaks: Q_{tr}^{-1}, Q_{PT}^{-1} and Q_{int}^{-1}. The Q_{tr}^{-1} is a transitory term which is strong for low frequencies (∼1 Hz) and when $\dot{T}$ is different from zero as applies to our experiments.

The second term Q_{PT}^{-1} is the internal friction due to the phase transition (PT) process, does not depend on $\dot{T}$. The third term Q_{int}^{-1} gives the intrinsic IF contribution characteristic of each phase (austenite, R-phase and martensite)

and only depends on their microstructure. Q_{PT}^{-1} and Q_{int}^{-1} play a more important role at high frequencies and can be ignored for the low frequency used.

The Q_{tr}^{-1} has a close relation to the model developed by Delorme [59], in which the internal friction of martensitic tranformation at a constant heating or cooling rate can be expressed as:

$$Q_{tr}^{-1} = \frac{1}{\omega} \frac{d\psi\left(V_m\right)}{dV_m} \frac{d\left(V_m\right)}{dt} \frac{dV_m}{dT} \frac{dT}{dt} \tag{1}$$

where V_m is the volume fraction of martensite, ω is the angular frequency and $\psi\left(V_m\right)$ is a monotonous function associated with transformation volume change or shape strain, which is assumed to be constant. Therefore Q_{tr}^{-1} should be proportional to the amount of martensite formed by unit of temperature, inversely proportional to the frequency, proportional to the cooling or heating rate and independent of measurement's amplitude. Using this approach, there is a linear relation between the internal friction Q_{tr}^{-1} and the term $\frac{\dot{T}}{f}$, where $\dot{T} = \frac{dT}{dt}$ is the heating and cooling rate and f is the frequency of vibration.

Thus, in the short form, the transitory part can be written as:

$$Q_{tr}^{-1} \approx \frac{\partial V_m}{\partial T} \frac{\dot{T}}{f} \tag{2}$$

Figures 7a-d show the influence of frequency and heating/cooling rate on the transformation peaks (P_R, P_M and P_A) and P_{rel} peaks. The results obtained are in agreement with predictions of equation (2) because internal friction decreases with increasing frequency (Fig. 7a-b) and increases with increasing temperature rate $\dot{T}$ (Fig. 7c-d). Figure 8 shows the dependence of this term for peaks P_R, P_M, and P_A with the heating/cooling rate. The plot shows that the internal friction does not vary linearly with heating rate as predicted by the

Delorme model, but the dependence seems to be logaritmic. The non-linear dependence of IF on $\dot{T}$ has also been observed by other investigators [60–63] and such a discrepancy can be explained by the modified transitory part by Gremaud *et al.* [64] later extended by Zhang *et al.* [63]. All transition temperatures were observed to be independent of the frequency and the temperature rate suggesting that the transformations involving change in crystal structure require very little thermal activation energy.

The relaxation peak at about 200 K (P_{rel}) shown in Figs. 6 and 7 in our materials has also been observed by Hasiguti and Iwasaki on equiatomic NiTi annealed at 1073 K and 873 K followed by furnace cooling [32]. They observed that the peak is reproducible between 100 and 473 K. On the other hand, Zhu and Gotthardt [33] observed the relaxation peak is nearly absent after quenching from 1273 K and becomes more pronounced when the quenching temperature is lower or when the samples were annealed between 673 and 923 K. Our results presented in Figure 7 are in a good agreement with previous findings [30, 32], where the peak temperature shifts to higher temperature with increasing frequency indicating that P_{rel} is thermally activated.

5 Conclusion

The transformation behaviour of NiTi particulates embedded in AA2124 matrix have been systematically studied by using DSC, TEP and internal friction. The following results have been established:

(1) The presence of NiTi particulates enhances the precipitation kinetics and damping capacity of the AA2124 matrices compared to that of unrein-

forced AA2124.

(2) Heat treatment performed at 768 K for 1 hour produces a two-step transformation (A→R→M) on cooling, while on heating only single M→A transformation occurs. Further aging at 463 K does not produce a remarkably difference in transformation temperatures. Aging at 463 K is too low to allow $Ti_{11}Ni_{14}$ to precipitate out within NiTi particulates.

(3) The martensitic transformation is affected by the applied vibration frequency and heating/cooling rate $\dot{T}$, however, the relation is not linear as predicted by Delorme's theory.

(4) The presence of Al in the NiTi particulates affects the transformation by broadening the R-phase transformation regime. The effect of Al on depressing M_s is not obvious as M_s is independent of the Ni/Ti ratio far away from the 50:50 ratio.

Acknowledgements

Robert Schaller and co-workers for building the IF instrument to our specs and introduction to this field, financial support via MicroNed research program workpackage I-C-4 is gratefully acknowledged.

References

[1] I. A. Ibrahim, F. A. Mohammed, E. J. Lavernia, J. Mater. Sci. 26 (1991) 1137-1156.

[2] T. S. Srivatsan, E. J. Lavernia, J. Mater. Sci. 27 (1992) 5965-5981.

[3] Z. G. Wei, C. Y. Tang, W. B. Lee, L. S. Cui, D. Z. Yang, Mater. Lett. 32 (1997) 313.

[4] J. N. Wei, H. F. Cheng, Y. F. Zhang, F. S. Han, Z. C. Zhou, J. P. Shui, Mater. Sci. Eng. A 325 (2002) 444.

[5] D. L. Davidson, Eng. Fract. Mech. 33 (1989) 965.

[6] D. L. Davidson, Metall. Trans. A 22 (1991) 97.

[7] K. Hamada, J. H. Lee, K. Mizuuchi, M. Taya, K. Inoue, Mat. Res. Soc. Symp. 459 (1997) 143-148.

[8] J. H. Lee, K. Hamada, K. Miziuuchi, M. Taya, K. Inoue, Mat. Res. Soc. Symp. 459 (1997) 419-424.

[9] Y. Furuya, A. Sasaki, M. Taya, Mater. Trans. JIM 34 (1993) 224-227.

[10] K. Hamada, J. H. Lee, K. Mizuuchi, M. Taya, K. Inoue, Metall. Mater. Trans. A 29 (1998) 1127.

[11] G. A. Porter, P. K. Liaw, T. N. Tiegs, K. H. Wu, Mater. Sci. Eng. A 314 (2001) 186.

[12] G. A. Porter, P. K. Liaw, T. N. Tiegs, K. H. Wu, JOM (2000) 52-56.

[13] A. Shimamoto, M. Taya, Trans. JSME 63 (1997) 26.

[14] K. A. Tsoi, R. Stalmans, M. Wevers, J. Schrooten, Y. X. Mai, Proc. SPIE 4234 (2001) 125-133.

[15] Y. Furuya, M. Taya, Trans. JIM 60 (1996) 1163.

[16] A. Shimamoto, H. Y. Zhao, H. Abe, Intl. J. Fatigue 26 (2004) 533.

[17] A. Shimamoto, Y. Furuyama, H. Abe, Key Eng. Mater. 334-335 (2007) 1093.

[18] G. M. Loughran, T. W. Shield, P. H. Leo, Intl. J. Solid Struct. 40 (2003) 217.

[19] W. Huang, Mater. Design 23 (2002) 11.

[20] K. H. Eckelmeyer, Scripta Metall. 10 (1976) 667-672.

[21] C. M. Hwang, M. Meichle, M. B. Salamon, C. M. Wayman, Philos. Mag. A 47 (1983) 9-30.

[22] I. Yoshida, T. Ono, M. Asai, J. Alloys and Compd. 310 (2000) 339-343.

[23] I. Yoshida, S. Yoshida, Sol. State Phenom. 89 (2003) 315-320.

[24] T. Kurita, H. Matsumoto, K. Sakamoto, K. Tanji, H. Abe, J. Alloy and Compd. 396 (2005) 193-196.

[25] H. Matsumoto, H. Ishiguro, J. Less Common Met. 153 (1989) 57-63.

[26] H. Matsumoto, Physica B 160 (1989) 138-142.

[27] J. Khalil-Allafi, A. Dlouhy, G. Eggeler, Acta Mater. 50 (2002) 4255-4274.

[28] G. Eggeler, J. Khalil-Allafi, S. Gollerthan, C. Somsen, W. Schmahl, D. Sheptyakov, Smart Mater. Struct. 14 (2005) 186-191.

[29] K. Wada, Y. Liu,J. Alloy Compd. 400 (2005) 163-170.

[30] J. S. Zhu, R. Schaller, W. Benoit, Phys. Lett. A 141 (1989) 177-180.

[31] J. Y. Lee, G. C. McIntosh, A. B. Kaiser, Y. W. Park, M. Kaack, J. Pelzl, K. Nahm,J. Appl. Phys. 89 (2001) 6223-6227.

[32] R. R. Hasiguti, K. Iwasaki, J. Appl. Phys. 39 (1968) 2182-2186.

[33] J. S. Zhu, R. Gotthardt, Phys.Lett. A 132 (1988) 279-282.

[34] S. A. Shabalovskaja, A. I. Lotkov, I. I. Sasovskaja, A. G. Narmonev, A. I. Zakharov, Solid State Commun. 32 (1979) 735-738.

[35] W. D. Armstrong, T. Lorentzen, Metall. Mater. Trans. A 33 (2002) 3535-3539.

[36] C. L. Xie, M. Hailat, X. Wu, G. Newaz, M. Taya, B. Raju, J. Eng. Mater. Technol. (Trans. ASME) 129 (2007) 69-76.

[37] D. D. Risanti, P. E. J. Rivera Díaz del Castillo, S. van der Zwaag, in: International Conference on Aluminium Alloys 11 Proceeding, Wiley VCH-Weinheim, 2008.

[38] J. M. Papazian, Metall. Mater. Trans. A 19 (1988) 2945-2953.

[39] M. P. Thomas, J. E. King, J. Mater. Sci. 29 (1994) 5272-5278.

[40] H. C. Shih, N. J. Ho, J. C. Huang, Metall. Mater. Trans. A 27 (1996) 2479-2494.

[41] J. M. Pelletier, R. Borrelly, Mater. Sci. Eng. 55 (1982) 191-202.

[42] J. M. Pelletier, G. Vigier, J. Merlin, P. Merle, F. Fouquet, R. Borrelly, Acta Metall. 32 (1984) 1069-1078.

[43] D. Sun, X. C. Sun, D. O. Northwood, J. H. Sokolowski, Mater. Charact. 36 (1996) 83-92.

[44] X. Kleber, L. Simonet, F. Fouquet, Modell. Simul. Mater. Sci. Eng. 14 (2006) 21-31.

[45] L. Parrini, R. Schaller, Acta Metall. Mater. 43 (1995) 2149-2156.

[46] S. Miyazaki, Y. Igo, K. Otsuka, Acta Metall. 34 (1986) 2045-2051.

[47] H. C. Lin, S. K. Wu, T. S. Chou, J. Alloys and Compd. 355 (2003) 90-96.

[48] T. Christman, S. Suresh, Acta Metall. 36 (1988) 1691-1704.

[49] I. Dutta, S. M. Allen, J. L. Hafley, Metall. Mater.Trans. A 22 (1991) 2553-2563.

[50] K. K. Chawla, A. H. Esmaeili, A. K. Datye, A. K. Vasudevan, Scripta Metall. Mater. 25 (1991) 1315-1319.

[51] C. S. Park, C. H. Kim, M. H. Kim, C. Lee, Mater. Chem. Phys. 88 (2004) 46-52.

[52] T. R. McNelly, P. N. Kalu, Scripta Metall. Mater. 25 (1991) 1041-1046.

[53] A. Somoza, M. Petkov, K. Lynn, A. Dupasquier,Phys. Rev. B 65 (2002) 094107-1-6.

[54] A. Nowick, B. Berry, Anelastic Relaxation in Crystalline Solids, Academic Press, 1972.

[55] W. Tang, B. Sundman, R. Sandström, C. Qiu, Acta Mater. 47 (1999) 3457-3468.

[56] S. F. Hsieh, S. K. Wu, J. Mater. Sci. 32 (1997) 989-996.

[57] S. Miyazaki, C. M.Wayman, Acta Metall. 36 (1988) 181-192.

[58] S. Miyazaki, K. Otsuka, Metall. Trans. A 17 (1986) 53-63.

[59] J. F. Delorme, R. Schmid, M. Robin, P. Gobin, J. de Physique Colloq. 32 (1971) 101-111.

[60] J. S. Zhu, R. Schaller, W. Benoit, Phys. Stat. Sol. A 108 (1988) 613-618.

[61] H. C. Lin, S. K. Wu, M. T. Yeh, Metall. Trans. A 24 (1993) 2189-2194.

[62] J. E. Bidaux, R. Schaller,W. Benoit, Acta Metall. 37 (1989) 803-811.

[63] J. X. Zhang, P. C. W. Fung, W. G. Zeng, Phys. Rev. B 52 (1995) 268-277.

[64] G. Gremaud, J. E. Bidaux, W. Benoit, Helv. Physica Acta 60 (1987) 947-958.

Table 1

Composition of AA2124 powder

Element	Cu	Mg	Mn	Fe	Si	Al
Wt.%	3.93	1.41	0.64	0.0624	0.21	Balance

Table 2. Transition temperatures evaluated from DSC data. A, R and M denote the austenitic, R-phase and martensitic transformation, respectively. Subscripts s, p and f refer to start, peak and finish, in the order mentioned.

Condition	NiTi vol.%	A_s (K)	A_p (K)	A_f (K)	$\Delta H_{A\rightarrow M}$ (J/g)	R_s (K)	R_p (K)	R_f (K)	M_s (K)	M_p (K)	M_f (K)	$\Delta H_{M\rightarrow A}$ (J/g)
SOL	10%	295	305	314	4.0	317	305	290	269	261	258	3.5
	20%	300	307	315	7.3	317	307	294	272	263	258	7.3
AGED	10%	290	304	310	2.4	298	290	282	268	258	244	2.6
	20%	297	305	310	6.2	298	290	282	272	264	252	6.5

Table 3

Transition temperatures evaluated from TEP data. A_s,A_f, M_s and M_f denote the austenitic and martensitic start and finish temperatures, respectively.

Condition	NiTi vol.%	A_s (K)	A_f (K)	M_s (K)	M_f (K)
SOL	10%	302	319	270	258
	20%	310	327	280	262
AGED	10%	300	312	275	252
	20%	302	318	275	250

Table 4

Transition temperatures evaluated from IF spectra. A_p, R_p, M_p, Rel_c and Rel_h denote the austenitic, R-phase, martensitic and relaxation (upon cooling/heating) peak temperatures, respectively.

Condition	NiTi vol.%	R_p (K)	M_p (K)	Rel_c (K)	Rel_h (K)	A_p (K)
SOL	10%	310	262	218	216	309
	20%	290	272	219	220	312
AGED	10%	297	264	220	227	314
	20%	290	263	219	225	308

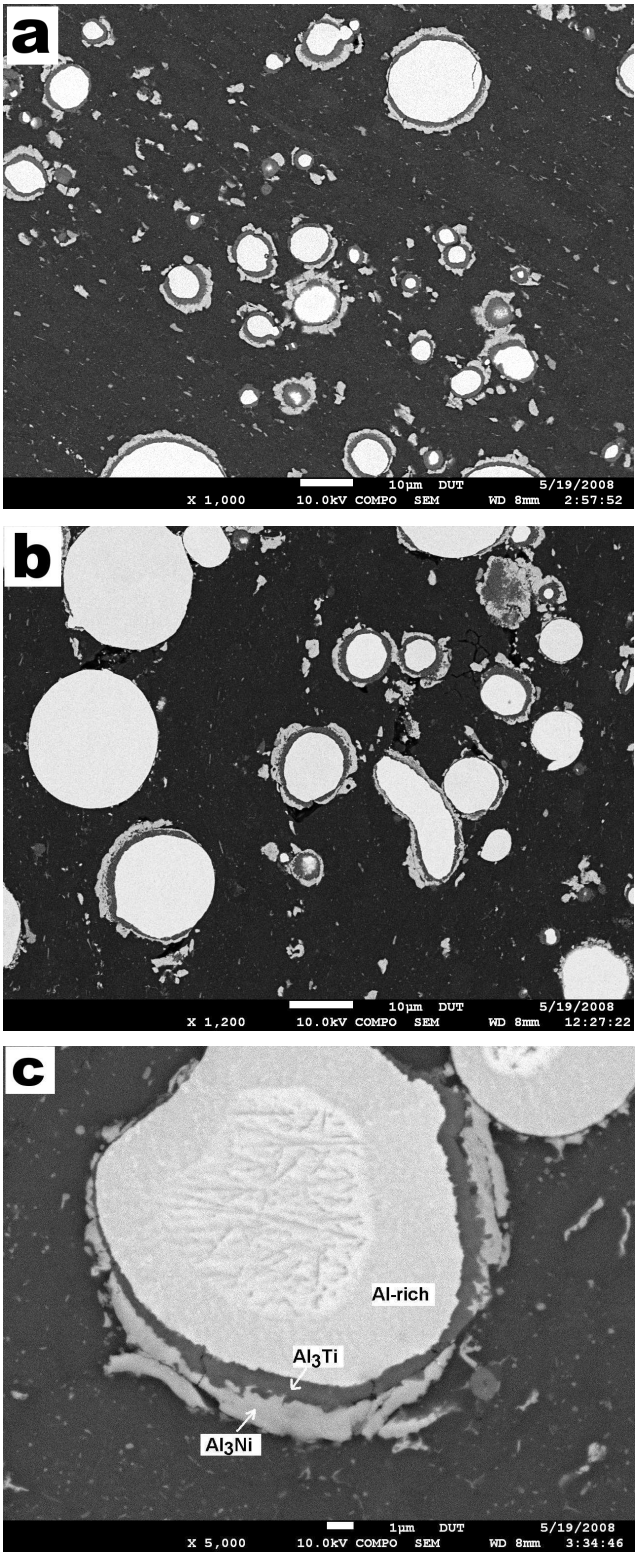

Fig. 1. Backscatter electron images of as received composites: (a) 10%, (b) 20% NiTi and (c) detailed interfacial microstructure of the NiTi/AA2124 composite.

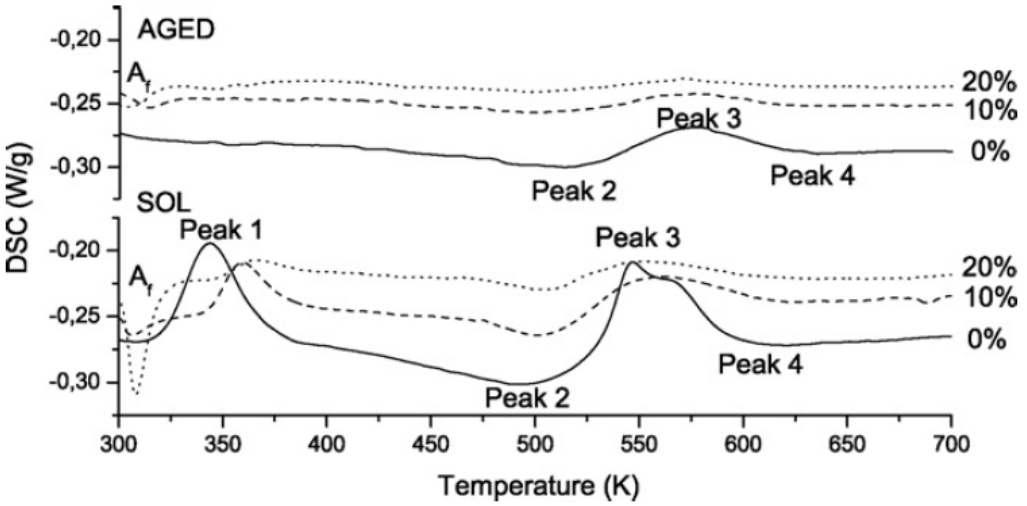

Figure 2. DSC thermograms recorded after SOL and AGED treatments. The amount of NiTi particulates is indicated. The curves have been offset for clarity.

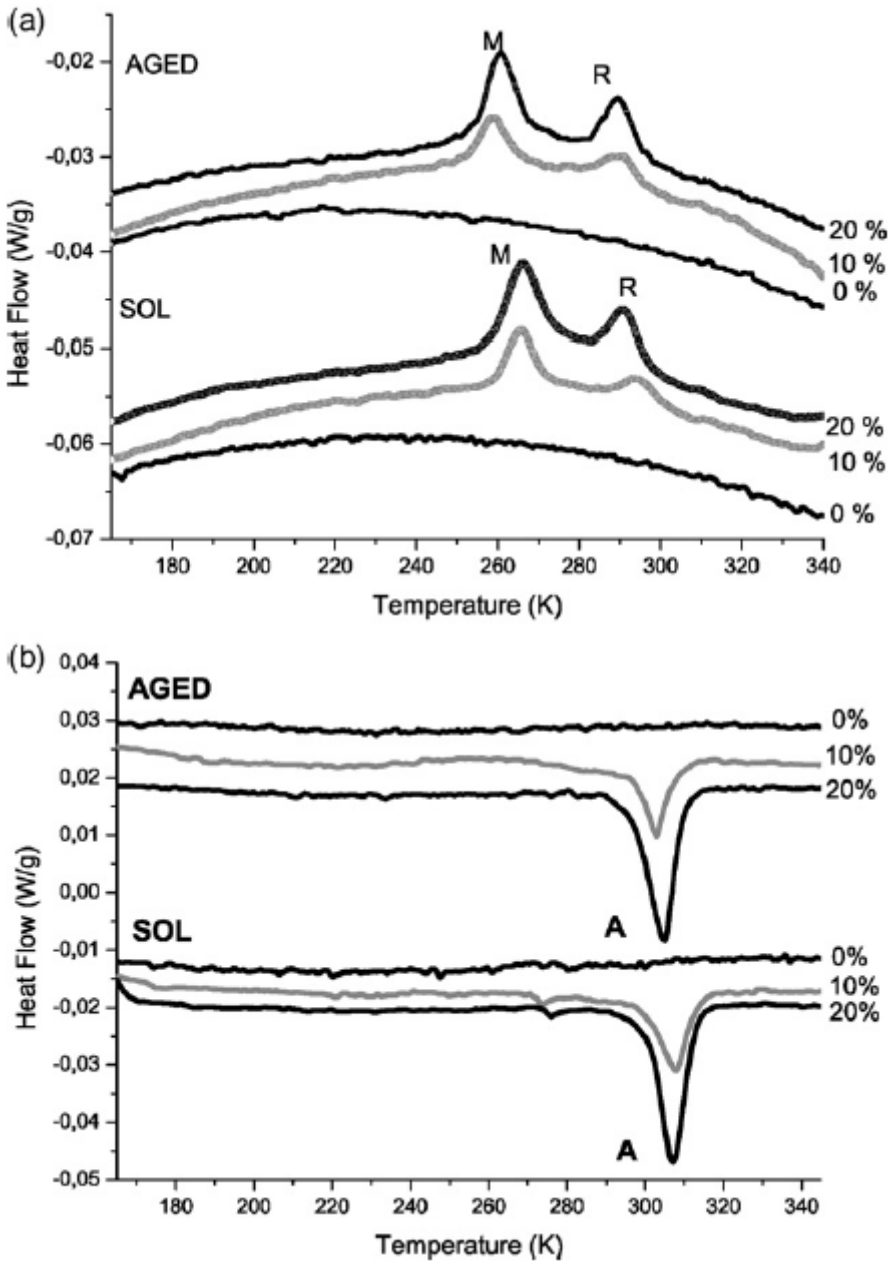

Figure 3 DSC thermograms recorded between 350K and 100K after SOL and AGED treatments: (a) on cooling and (b) on heating. The amount of NiTi particulates is indicated. The curves have been offset for clarity.

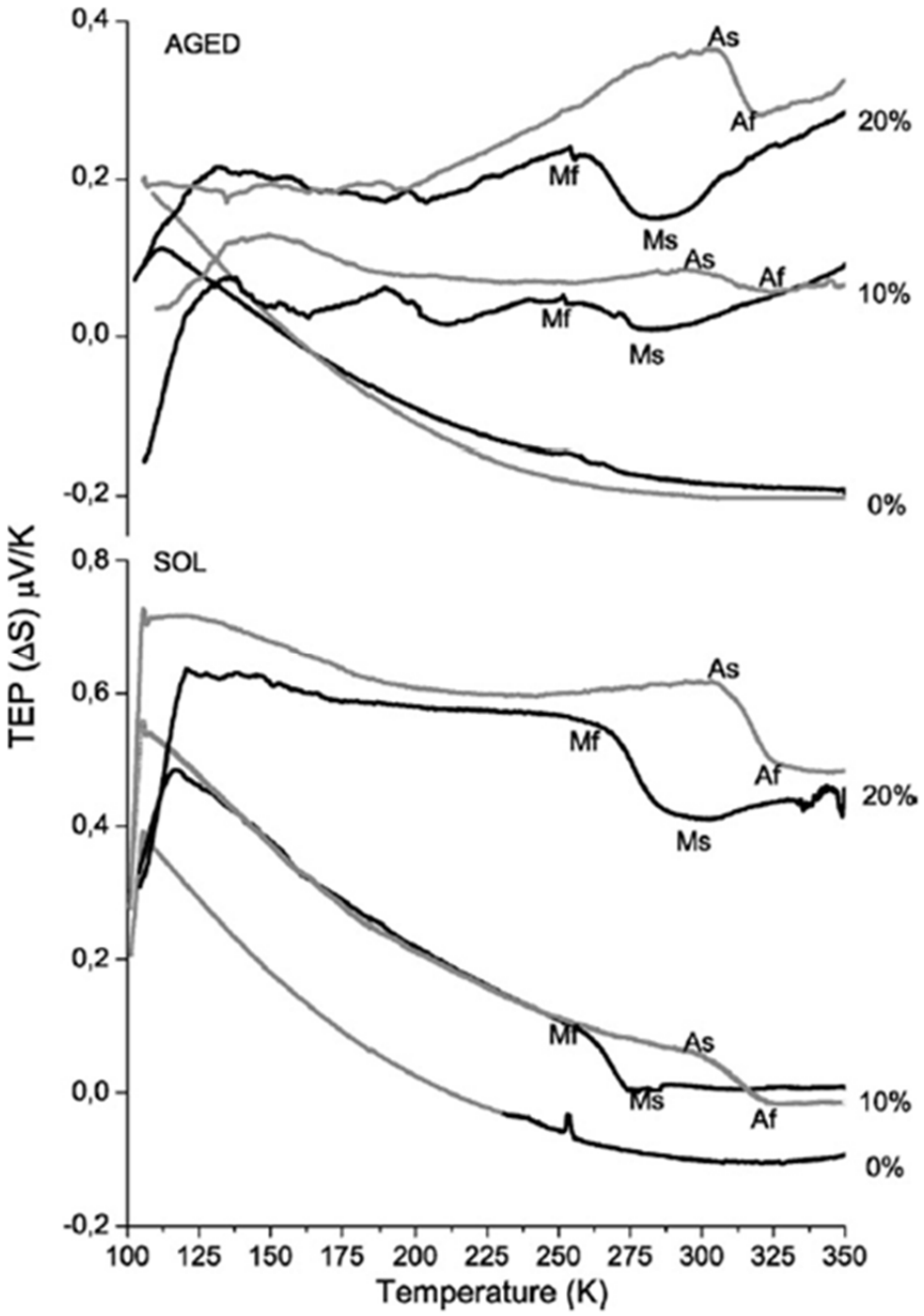

Figure 4 Thermoelectric power datameasured between 350K and 100K after SOL and AGED treatment. The amount of NiTi particulates is indicated. Black and grey lines indicate data collected upon cooling and heating, respectively.

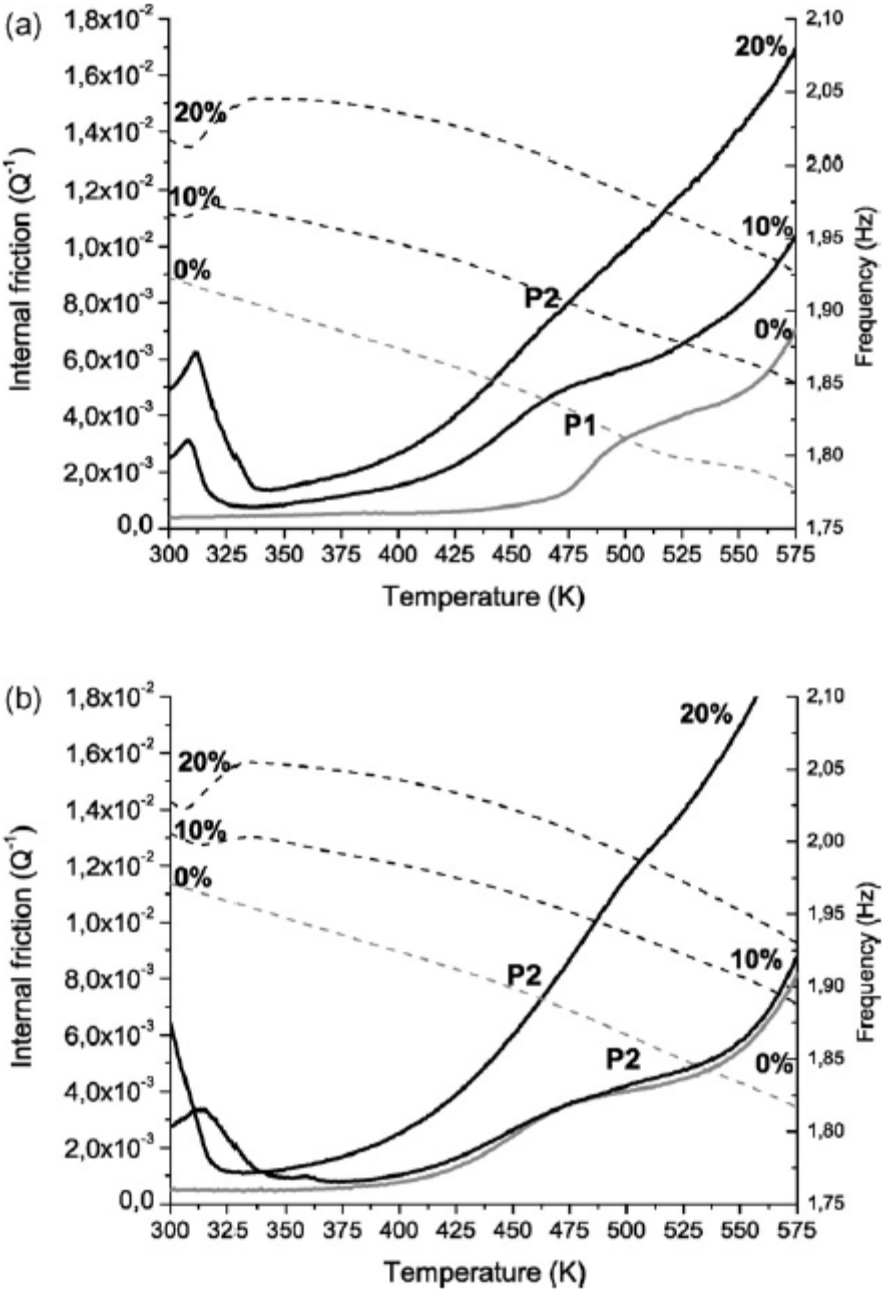

Figure 5 Internal friction spectra (solid lines) and its respective frequency variation (dashed lines) recorded between 300K and 600K: (a) SOL and (b) AGED. The amount of NiTi particulates is indicated.

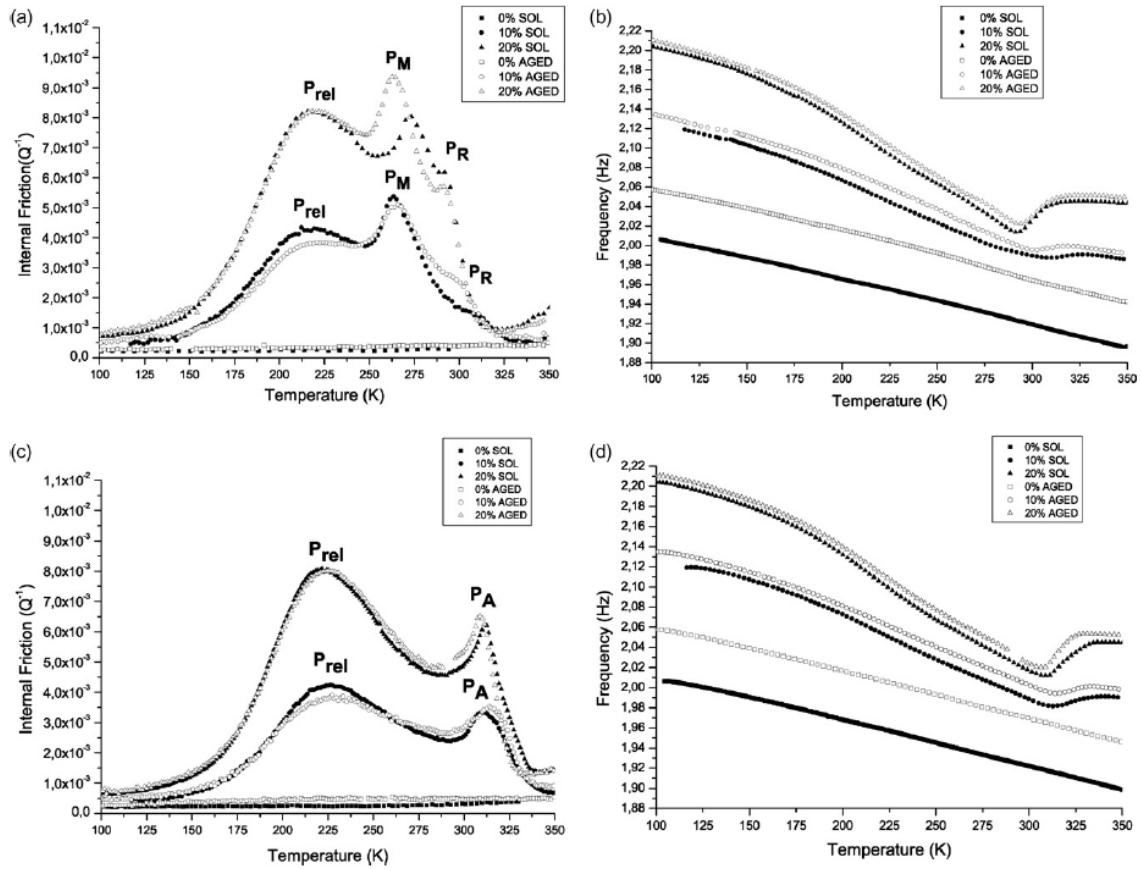

Figure 6 Internal friction spectra and its respective frequency variation recorded between 350K and 100K: (a and b) upon cooling and (c and d) upon heating. P_A, P_R, P_M and P_{rel} denote peak associated to M→A, A→R, R→M and relaxation, respectively.

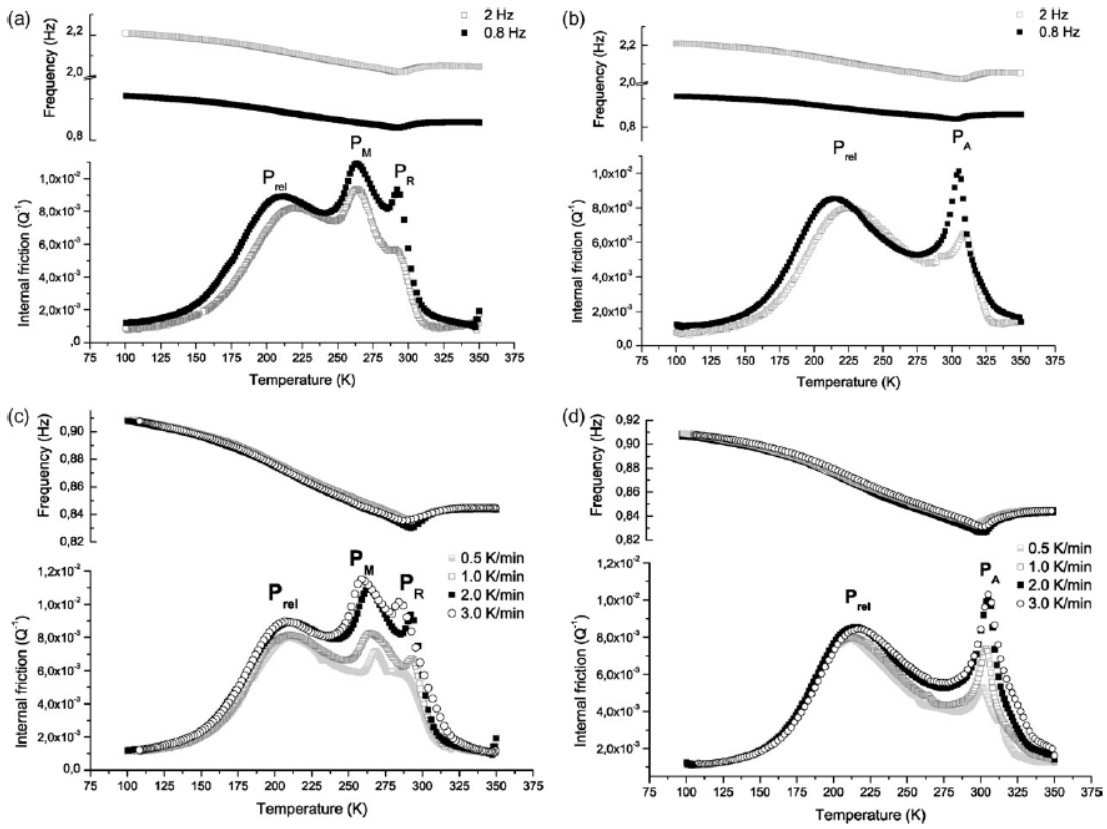

Figure 7 Internal friction spectra and its respective frequency and temperature rate variation of 20% NiTi composite in AGED state. Data were recorded between 350K and 100K: (a) frequency variation upon cooling, (b) frequency variation upon heating, (c) temperature rate variation upon cooling and (d) temperature variation upon heating. P_A, P_R, P_M and P_{rel} denote peak associated to M→A, A→R, R→M and relaxation, respectively. Variation in frequency and temperature rate are indicated in the figure.

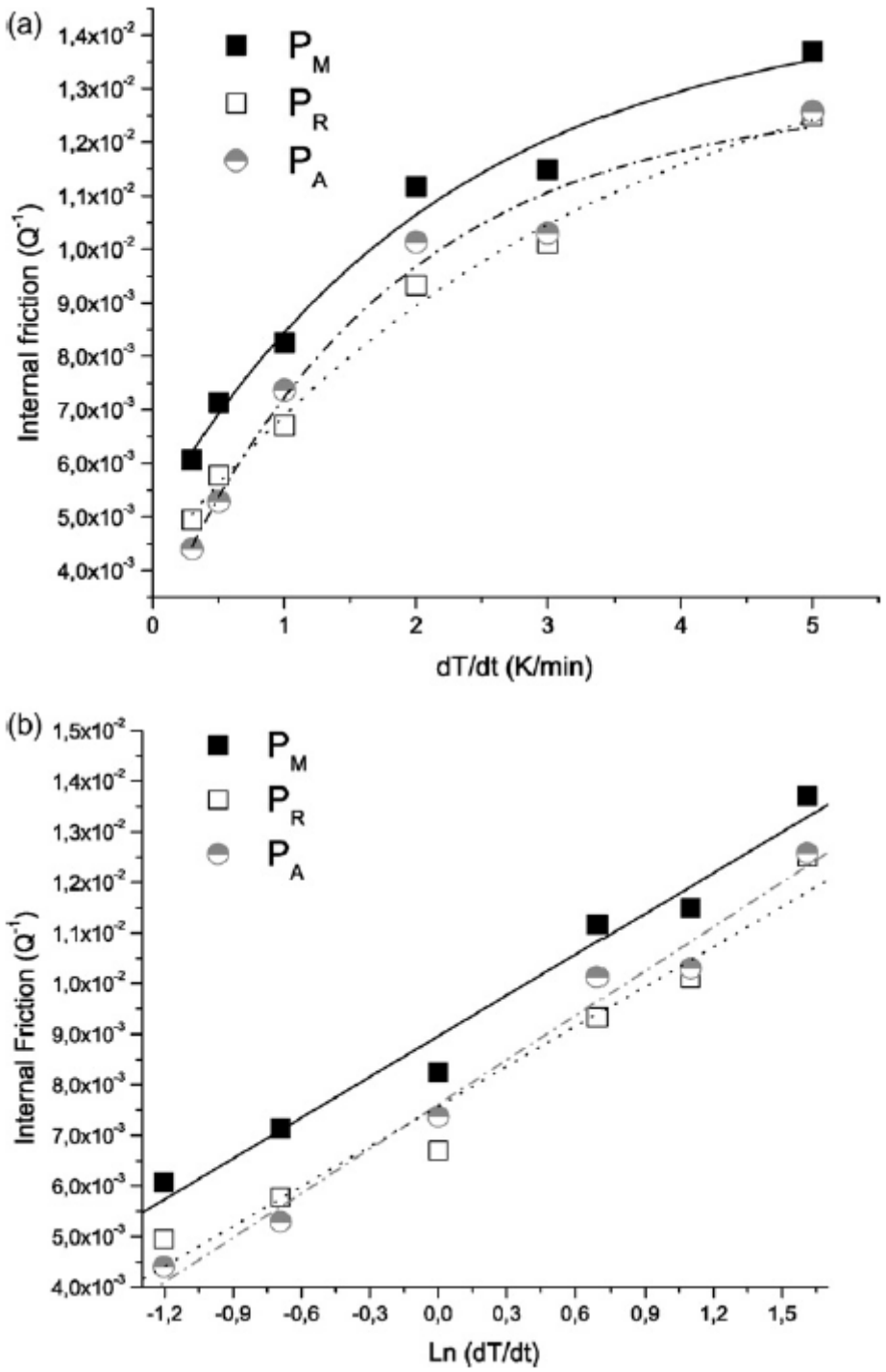

Figure 8 Internal friction spectra of 20% NiTi composite in AGED condition as function of dT/dt at frequency of 0.8 Hz. Peaks associated to the transformations are indicated in the figure: (a) non-linear relation and (b) fitted to linear relation of Q^{-1} = A ln(1 + B(dT/dt)/f).